Films of a disk-shaped liquid crystalline molecule—DNA complex at interfaces

K. A. Suresh[1] AND Alpana Nayak[2]

Abstract | In this review article, we describe the studies on disk-shaped (discotic) liquid crystalline molecule—DNA complex films at air–water (A–W) and air–solid interfaces. The interaction of DNA with molecules in a monolayer at A–W interface has drawn considerable attention in recent years to understand supramolecular organization as well as the transfer of DNA across biological membranes in gene therapy. We have formed films of a novel ionic discotic liquid crystalline molecule, pyridinium salt tethered with hexaalkoxytriphenylene (PyTp) and its complex with DNA (PyTp–DNA) at A–W interface. The PyTp b monolayer was formed on the aqueous subphase containing small amount of DNA. The electrostatic interaction between PyTp and DNA molecules results in a PyTp–DNA complex monolayer. Surface manometry and Brewster angle microscope studies of the PyTp–DNA complex monolayer film indicate the molecules to be in the edge-on configuration. The PyTp–DNA complex films were transferred onto silicon wafers using Langmuir–Blodgett (LB) technique. We find that several tens of layers of PyTp–DNA complex monolayer can be transferred with high efficiency. We also describe nanoscale electrical conductivity studies for the pure PyTp and PyTp–DNA complex LB films carried out using current-sensing atomic force microscope.

1. Introduction

The studies on the monolayer films of disk-shaped (discotic) molecules at air–water interface (Langmuir films) and air–solid interface (Langmuir–Blodgett films) have become very important[1–3]. Thin films of discotic liquid crystalline molecules (mesogens) have technological applications in the fabrication of gas sensors[4], field-effect transistors[5], photovoltaic diodes[6], solar cells and optical displays[7]. In addition, these systems have helped in modeling of $\Pi-\Pi$ and steric interactions in biological systems[8,9]. Disk-like molecules, like porphyrins, vitamins and so on, play a significant role in living systems. At air–water (A–W) interface, discotic mesogens can self-assemble into one-dimensional columnar superstructures due to the overlapping of Π-orbitals of adjacent molecules, thereby forming stable monolayers. Such monolayers formed by amphiphilic molecules at A–W interface are called Langmuir monolayers. These films transferred onto solid substrates are called Langmuir–Blodgett (LB) films[3,10]. These films need to be transferred to solid supports for practical applications. The preparation of ultra thin films by means of LB technique is an efficient method to obtain highly ordered layers over large areas[11]. LB films of discotic mesogens have been reported to have a surface morphology which are periodically modulated by columns that tend to lie along the film deposition direction[1]. Compared to the conventional discotic liquid crystals, ionic discotic mesogens are unique and exploit the properties of

[1]*Centre for Liquid Crystal Research, P.B.No. 1329, Jalahalli, Bangalore 560013, India*
[2]*Raman Research Institute, Sadashivanagar, Bangalore 560080, India*
suresh@clcr.res.in

liquid crystals and ionic liquids. This makes them promising candidates for designing anisotropic ion-conductive materials because of the anisotropic structural organization and the presence of ions as charge carriers[12–14].

Discotic mesogenic molecules possess unique molecular electronic properties, like two-dimensional delocalizations of electrons, which are not observed in linear oligomers and polymers[15]. In addition, these molecular electronic properties are amplified at the supramolecular level due to the extended interactions between Π-orbitals. Therefore, discotic mesogens are truly a new generation of organic semiconductors[16]. In addition, the DNA molecule has drawn lot of attention in nanoelectronic devices due to its intrinsic electronic properties[17–19]. Since both DNA and discotic mesogens have their own intrinsic electronic properties, complexing DNA with cationic discotic mesogens molecules is a novel approach for developing advanced materials with interesting electronic properties[20,21]. A variety of cationic surfactants, such as linear and branched polymer, glycopeptides, dendrimers, and lipid membranes, have been shown to form complexes with DNA[22–24]. LB films are also useful for the immobilization of nucleic acids (DNA, polynucleotides) on solid supports in the designing of nucleic acid-based biosensors[25]. Although there have been many studies on the formation of DNA–cationic lipid complexes[26], there have been no reports on the interaction of DNA with cationic discotic molecules at the A–W interface.

In this article, we review our studies on the films of a cationic discotic mesogen, pyridinium tethered with hexaalkoxytriphenylene with bromide counter-ion (PyTp) and its complex with DNA (PyTp–DNA) at both A–W and air–solid (A–S) interfaces[27,28]. We find that, at A–W interface, the PyTp–DNA complex monolayer exhibits a higher collapse pressure, compared to the pure PyTp monolayer, indicating better stability. Using LB technique, we have transferred these films onto solid substrates. We find that the formation of the DNA complex enhanced the transfer efficiency over several tens of layers.

We have carried out electrical conductivity measurements at nanoscale on the LB films of both pure PyTp and PyTp–DNA complex employing current-sensing atomic force microscope (CS-AFM)[29]. CS-AFM provides an attractive method to make electrical contacts with the monolayer films under controlled load and to form metal–molecule–metal junction[30–32]. The conventional CS-AFM operates in contact mode. For soft systems, the damage due to lateral shear forces in contact mode

imaging is an important issue. However, for systems like self assembled monolayer and polymers, the contact mode can still be used[33,34]. The ability to rationally design molecular electronic components hinges on a fundamental understanding of the charge transport mechanism in metal–molecule–metal junctions[35]. Hence, we look for a possible mechanism for electron transport at such a junction in our system. The analysis of the current–voltage ($I–V$) characteristics obtained for the pure PyTp film and the PyTp–DNA complex film suggests electron tunneling to be a possible charge transport mechanism in our system.

2. Experimental

The material PyTp was synthesized by Sandeep Kumar and Santanu K. Pal[36]. The surface manometry experiments were carried out using a NIMA 611M Langmuir trough. A schematic diagram of the Langmuir trough is shown in Figure 1. The subphase used was ultrapure deionized water (pH 5.8) obtained from Millipore Milli-Q system. The surface pressure (π)–area per molecule (A_m) isotherms were obtained by symmetric compression of the barriers with a constant compression rate of 0.1 nm^2/molecule/min. The surface pressure (π) was measured using the standard Wilhelmy plate technique. The nature of the π–A_m isotherm indicates the monolayer phases and their phase transitions. For complexation with DNA, sodium salt of DNA (Sigma) was dissolved in the ultrapure water subphase. This is a double-stranded DNA from Salmon testes with approximate molecular weight of 1.3×10^6 (∼2000 bp). The π–A_m isotherm for the complex monolayer was obtained by spreading the solution of PyTp on the subphase containing DNA at various concentrations.

A Brewster angle microscope (BAM), MiniBAM (NFT, Nanotech, Germany) was employed to observe the films at the A–W interface. Figure 2 illustrates the principle of image formation using a BAM. Using BAM, one can study the phase transitions in a monolayer film at A–W interface by observing in situ changes in morphology of the film during compression or expansion.

Langmuir–Blodgett (LB) technique was employed to transfer various layers onto hydrophilic and hydrophobic substrates at different target surface pressures (π_t). A surface pressure value that is maintained constant by adjusting the area per molecule during a film transfer to a substrate is called target surface pressure. A schematic diagram of the LB technique is shown in Figure 3. To obtain hydrophilic surfaces, the polished silicon wafers were treated for about 5 min in hot piranha

Figure 1: A schematic diagram of the Langmuir trough and the setup for the measurement of surface pressure (π)–area per molecule (A_m) isotherm.
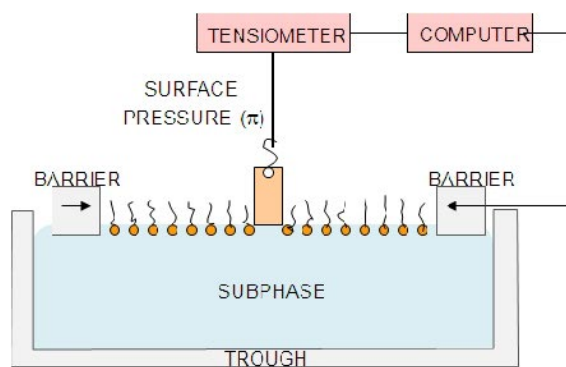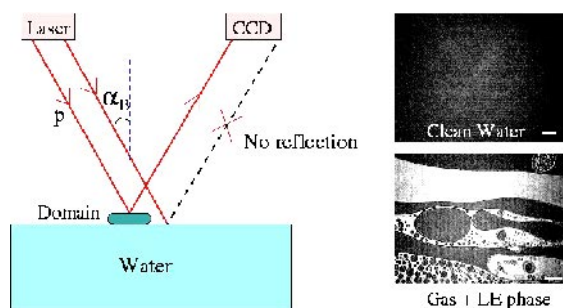

Figure 2: A schematic diagram showing the principle of image formation by a Brewster angle microscope (BAM), where α_B is the Brewster angle of water with respect to air. The top and bottom pictures on the right side show the BAM images obtained for clean water and a monolayer in the gas + liquid expanded coexistence phase respectively.

solution (mixture of concentrated H_2SO_4 and H_2O_2 in 3:1 ratio) which were then rinsed in ultrapure deionized water and later dried. For hydrophobic surfaces, clean silicon substrates were dipped in hexamethyldisilazane (HMDS) for 12 hours and then rinsed with HPLC grade chloroform. Horizontal deposition technique was used to obtain films on substrates at low π. A schematic diagram of the horizontal deposition technique is shown in Figure 4.

The atomic force microscope (AFM) studies on these LB films were performed using model PicoPlus (Molecular Imaging). AFM yields the morphology of the film on the air–solid (A–S) interface in the nanoscale. The topography of the films were obtained in the tapping mode AFM using silicon tips with spring constant of 21 N/m and resonance frequency of 250 kHz. A schematic diagram of an AFM setup in the tapping mode is shown in Figure 5. To obtain the thickness, the films were scratched with the same tip in contact mode.

The topography of the scratched region was imaged in the tapping mode.

For electrical conductivity measurements, we have formed the films on gold coated mica substrate. These substrates, obtained commercially, were rinsed with HPLC grade chloroform and dried before film deposition. The conductivity measurements were carried out using a contact mode CS-AFM. We have used platinum coated silicon cantilevers having spring constant in the range of 0.02 to 0.8 N/m, tip radius ~30 nm and resonance frequency in the range of 5 to 25 kHz for CS-AFM measurements. The deflection of the cantilever was monitored and kept constant to maintain a constant force between the tip and the sample during I-V measurements and current imaging.

3. Results and Discussion

The material PyTp exhibits the following liquid crystal phase sequence in the bulk: solid (S) -

Figure 3: Schematic diagram showing film deposition on a substrate by Langmuir–Blodgett (LB) technique. To form an LB film, the substrate is moved up and down vertically through the monolayer at an air–water interface a number of times. The surface pressure is maintained constant during monolayer transfer by moving the barriers of the Langmuir trough through feed back mechanism.
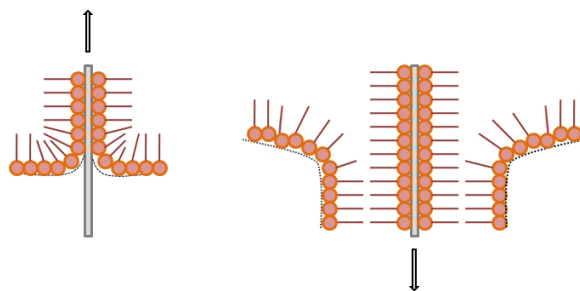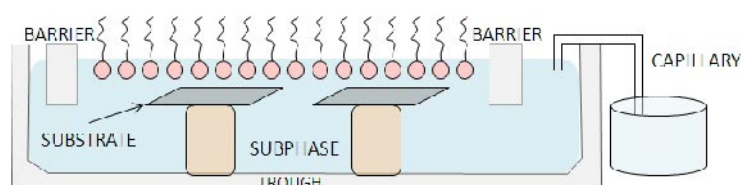
Figure 4: Schematic diagram of the horizontal deposition technique. This technique facilitates the deposition of Langmuir monolayer on hydrophilic substrates at low surface pressures at which Langmuir–Blodgett technique is not very efficient.

columnar phase (Col); 83.7°C, Col - isotropic; 95°C. On cooling, the isotropic phase transformed to columnar phase at 92°C that remained stable down to room temperature[36].

3.1. Surface Manometry

The surface pressure (π)–area per molecule (A_m) isotherm for the monolayer of PyTp molecule formed on ultrapure deionized water subphase is shown in Figure 6. The isotherm for pure PyTp shows a gradual rise in π up to 9 mN/m followed by a sharp rise and finally transforms to a collapsed state at a π of about 44 mN/m. In the collapsed state, instead of a uniform monolayer one has three dimensional crystallites or multilayers. The limiting area per molecule (A_o) values obtained by extrapolation to zero surface pressure were 1.15 nm^2/molecule at the steep increasing region and 3.1 nm^2/molecule at the gradual increasing region respectively. Figure 7 shows the molecular structure of PyTp according to standard bond lengths and angles. The computed surface area of the aromatic core is equal to 0.785 nm^2. The surface area occupied by the molecule increases to 4.5 nm^2 if the extended peripheral hydrocarbon tails are included. The observed A_o value for the first transformation

(3.1 nm^2/molecule) suggests an expanded phase, whereas for the second transformation, the observed A_o value (1.15 nm^2/molecule) suggests a condensed phase[27]. In literature[37,38], the expanded phase and the condensed phase of the monolayer are also referred as low density liquid and high density liquid respectively. The π–A_m isotherms for the PyTp molecule with different molar concentrations of DNA in the subphase are shown in Figure 8. The nature of the isotherm of the PyTp monolayer changes with the addition of DNA in the subphase. We find that, the collapse pressure increases and the A_o value of the isotherm decreases with the increase in the concentration of DNA in the subphase. However, beyond 10^{-8} M concentration of DNA, there was no further change in the isotherm. The decrease in the A_o value and the increase in the collapse pressure as compared to the pure PyTp monolyer indicates condensation and enhanced stability of the PyTp–DNA complex monolayer. For the 10^{-8} M concentration, the collapse pressure was about 58 mN/m, which is 25% higher as compared to the pure PyTp monolayer. The isotherm exhibited a clear slope change at 0.95 nm^2/molecule, indicating a phase transformation. The A_o value was 1.9 nm^2/molecule

Figure 5: A schematic diagram showing an atomic force microscope setup in the tapping mode.
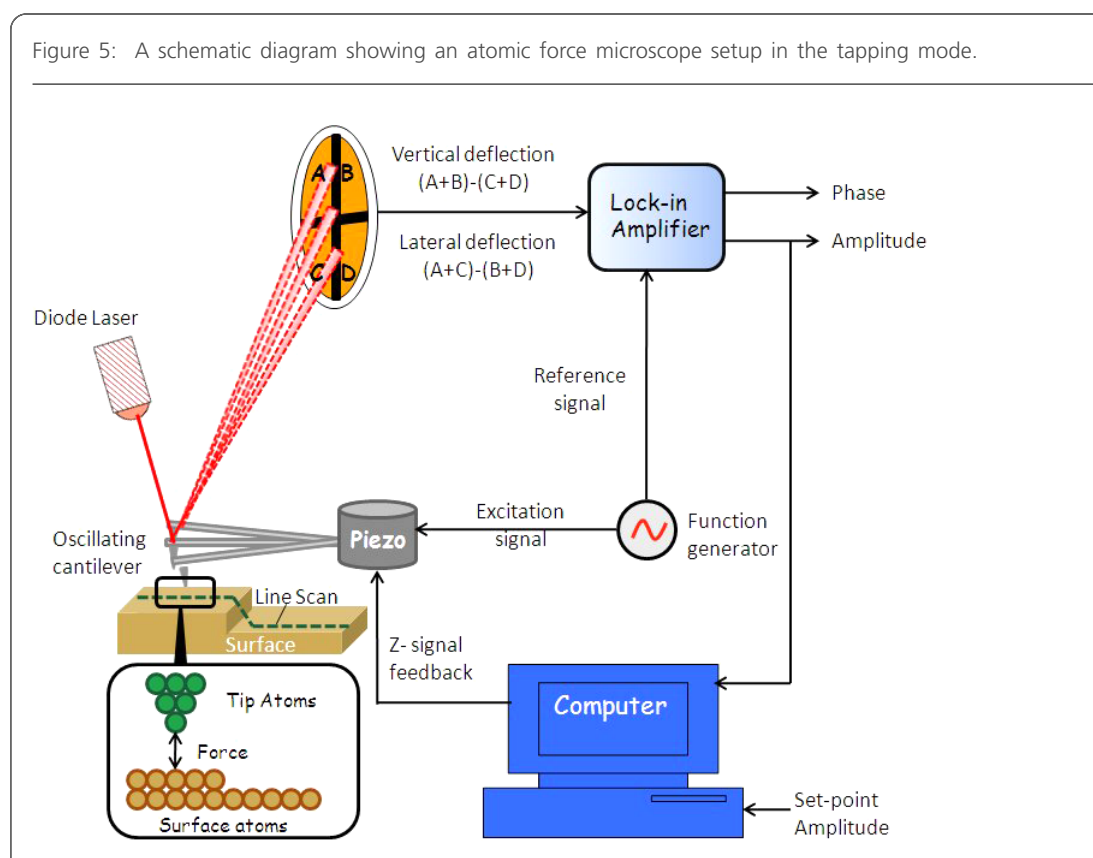
for the first transformation and 0.9 nm^2/molecule for the second transformation. Comparing with the molecular dimension, we suggest that the molecules adopt the edge-on conformation with a value of 1.9 nm^2/molecule, corresponding to an expanded phase, and a value of 0.9 nm^2/ molecule, corresponding to a condensed phase. The isotherm cycles performed by compression and expansion of the PyTp–DNA complex monolayer at the condensed phase showed a negligible amount of hysteresis. However, if the isotherm cycles were performed after the complex monolayer reached the collapsed state, an appreciable amount of hysteresis was observed, and the monolayer did not exhibit reversibility on expansion. This behavior was unlike the pure PyTp monolayer, which showed completely reversible collapse. This indicated a stable complex formation between DNA and the cationic PyTp molecules at the A–W interface[28].

The rigidity modulus of the films were calculated from the compressional elastic modulus, $|E|$ given by $|E| = A_m(d\pi/dA_m)$. The $|E|$ value characterizes the stability of a monolayer's phases[37]. Specifically, a maximum value of the $|E|$ in the range of 12.5 mN/m to 50 mN/m is characteristic of liquid expanded phase, whereas a value between 100 and 250 mN/m ischaracteristic of the liquid condensed phase[38]. The variation of $|E|$ with A_m obtained from the

isotherms of pure PyTp monolayer and PyTp–DNA complex monolayer are shown in Figure 9. The variation of $|E|$ with A_m showed a maximum of 83 mN/m at A_m of 0.871 nm^2/molecule for the pure PyTp monolayer, whereas, the $|E|$ value showed a maximum of 283 mN/m at an A_m of 0.78 nm^2/ molecule for the PyTp–DNA complex monolayer. Interestingly, the maximum $|E|$ value attained by the complex monolayer was more than three times the value attained by the pure PyTp monolayer, indicating a much better packing of molecules in the complex monolayer. We find a sharp change in the value of $|E|$ at an A_m of 0.95 nm^2/molecule for the complex monolayer, indicating a phase transition. The phase above an A_m of 0.95 nm^2/molecule has a much lower value of $|E|$ as compared to the phase below this A_m. This suggests that the complex monolayer undergoes a phase transition in the edge-on configuration from an expanded phase to a condensed phase[28].

3.2. Brewster Angle Microscopy

The BAM images of PyTp monolayer obtained during compression of the film at A–W interface are shown in Figure 10. It was observed that the intensity increases gradually upon compression from nearly zero surface pressure (Figure 10a). This transforms to 3D crystals (Figure 10b) in the

Figure 6: Surface pressure (π)–area per molecule (A_m) isotherm of pyridinium tethered with hexaalkoxytriphenylene (PyTp) molecule. The extrapolation to zero surface pressure, shown by dashed lines, gives the limiting area per molecule (A_o). The structure of the PyTp molecule is shown as an inset. [Reprinted with permission from reference 27. Copyright 2007 American Chemical Society].
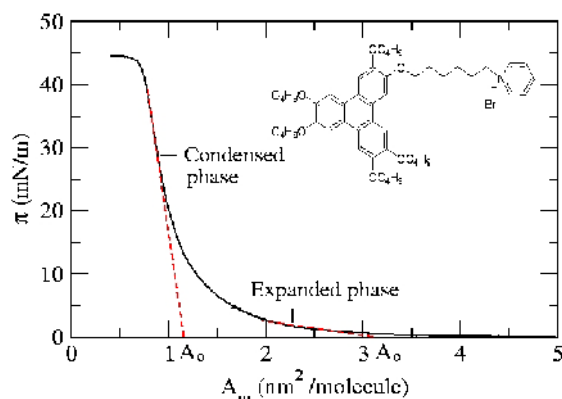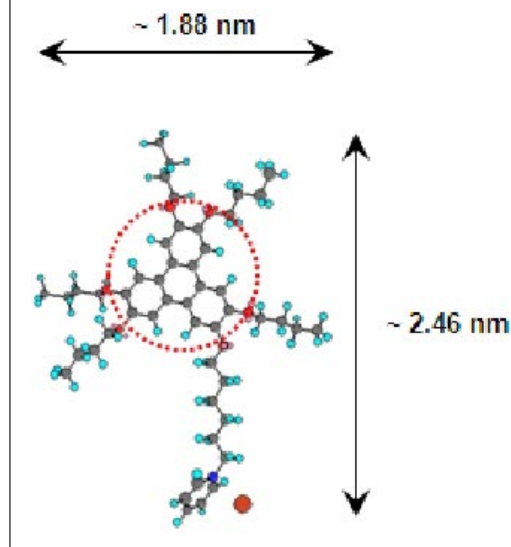
Figure 7: Molecular structure of PyTp according to the standard bond lengths and bond angles. The triphenylene disc area shown in dotted circle is about 0.785 nm².

collapsed state. On expansion, these crystalline domains disappeared, and the PyTp system reverted back to the uniform intensity region indicating a monolayer state. This observation confirms the reversibility of the PyTp film. The BAM images of the PyTp–DNA complex monolayer with 10^{-8}M concentration of DNA in the subphase are shown in Figure 11. Similar to the pure PyTp monolayer, the intensity in the BAM image of the PyTp–DNA complex film increases gradually upon compression (Figure 11a). But in the collapsed state, the 3D domains were markedly different. Pure PyTp film showed small crystalline domains filling the whole surface of water in a mesh-like texture. On the contrary, the PyTp–DNA complex film showed long, thread-like 3D domains (Figure 11b) after the collapse. On expansion, these thread-like domains continued without change, and the PyTp–DNA complex in the collapsed state did not revert back to its original monolayer state. These results, together with results from surface manometry, indicated the stable complex formation between the DNA molecules and the cationic discotic PyTp molecules at the A–W interface. Here, the interaction is mainly electrostatic between the pyridinium group of discotic mesogen and the phosphate group of DNA,

Figure 8: Surface pressure (π)–area per molecule (A_m) isotherms for the monolayer of PyTp–DNA complex for different concentrations of DNA in the subphase. [Reprinted with permission from reference 28. Copyright 2008 American Chemical Society].
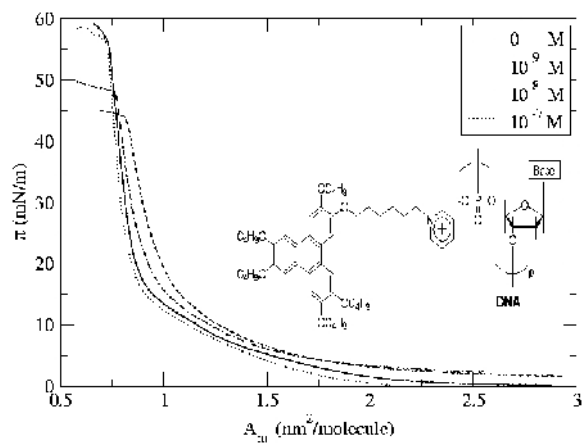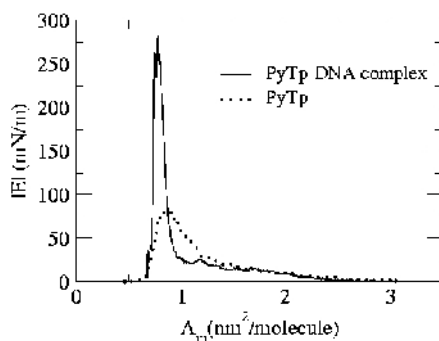

Figure 9: Variation of compressional elastic modulus (|E|) with area per molecule (A_m) for the pure PyTp monolayer (dotted line) and the PyTp–DNA complex monolayer (continuous line) with a 10^{-8} M concentration of DNA in the subphase. [Reprinted with permission from reference 28. Copyright 2008 American Chemical Society].

which play an important role in the formation and stability of the complex films[27,28].

3.3. Atomic Force Microscopy
3.3.1. Topography

The AFM topography images of the PyTp monolayer transferred in the expanded phase (5 mN/m) by horizontal method on a hydrophilic silicon substrate (Figure 12a) indicates that the height of the film is about 0.7 nm with reference to the substrate. This corresponds to the thickness of the molecules lying parallel to the A–S interface. When the monolayer was transferred in the condensed phase (35 mN/m) by LB technique (Figure 12b), the topography indicated a uniform and homogeneous film with a height of about 2 nm

with reference to the substrate. This corresponds to the thickness of the molecules lying normal to the A–S interface.

The π–A_m isotherm of PyTp (Figure 6) and its |E| values (Figure 9) imply a phase transformation from an expanded phase to a condensed phase. The A_o values obtained in the expanded phase was 3.1 nm^2/molecule and in the condensed phase was 1.15 nm^2/molecule. Also, the AFM topography images showed a height of about 0.7 nm for the PyTp film transferred in the expanded phase and a height of about 2 nm for the PyTp film transferred in the condensed phase. Comparing all these results with the molecular dimensions (Figure 7), we infer the molecules to have a face-on structure in the expanded phase and an edge-on structure in

Figure 10: BAM images of PyTp film formed on a subphase of ultrapure deionized water. (a) Condensed phase ($A_m = 1.2$ nm^2), (b) collapsed state ($A_m = 0.7$ nm^2) showing coexistence of 3D crystals and condensed phase. The scale bar in each image represents 500 μm. [Reprinted with permission from reference 27. Copyright 2007 American Chemical Society].
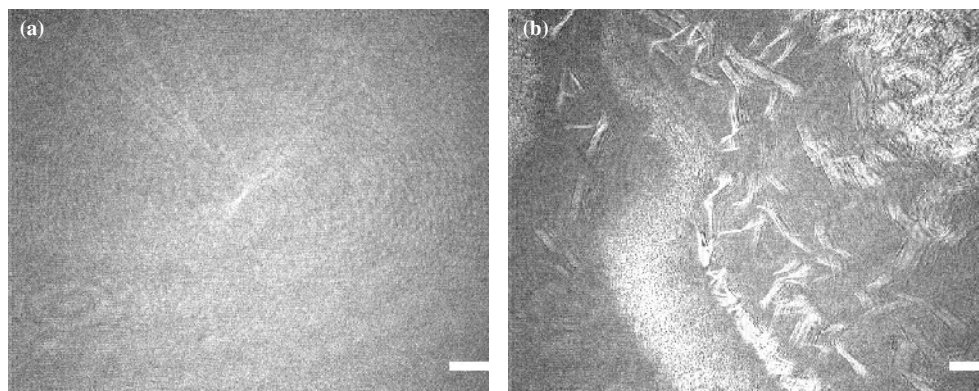

Figure 11: BAM images of PyTp–DNA complex film formed on a subphase containing 10^{-8} M concentration of DNA. (a) Condensed phase ($A_m = 0.85$ nm^2), and (b) collapsed state ($A_m = 0.35$ nm^2) showing coexistence of long thread-like 3D domains and condensed phase. The scale bar in each image represents 500 μm. [Reprinted with permission from reference 28. Copyright 2008 American Chemical Society].
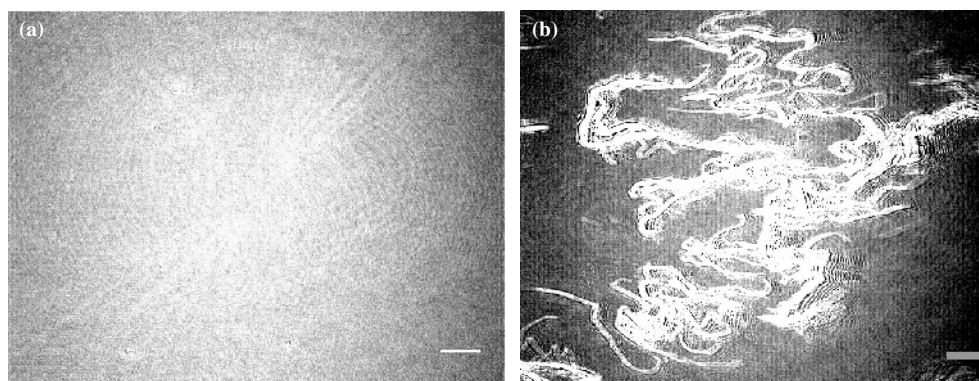
the condensed phase. This also indicates that the structure of the Langmuir films was maintained throughout the transfer process from the A–W interface to the A–S interface[39]. On the basis of these results, we represent the face-on and edge-on configuration at the A–W interface as shown in Figure 13. In our system, the presence of highly polar pyridinium moiety together with six oxygen atoms at the periphery of the triphenylene core have enhanced the hydrophilicity of the molecules, thereby facilitating the face-on configuration at large A_m values at the A–W interface.

The AFM image of the LB film of PyTp with two layers transferred onto hydrophobic silicon substrates at different target surface pressures (π_t)

are shown in Figure 14. The film with two layers at π_t of 35 mN/m (Figure 14a) and 42 mN/m (Figure 14b) revealed a morphology with narrow rectangular voids elongated in the direction of the film deposition. We find that with increasing value of π_t, the film coverage improves. At all these surface pressures, the height profiles of the images yield a value of about 4.0 ± 0.2 nm. This corresponds to the value of two layers of the molecules in the edge-on configuration.

The AFM images of the PyTp–DNA complex monolayer transferred onto hydrophilic silicon substrates are shown in Figure 15. The film transferred at a π_t of 5 mN/m (Figure 15a) showed a height of 1.4 ± 0.4 nm with reference to the

Figure 12: The AFM images of PyTp monolayer transferred onto hydrophilic silicon substrates at target surface pressures (π_t). A surface pressure value that is maintained constant by adjusting the area per molecule during a film transfer to a substrate is the target surface pressure. (a) $\pi_t = 5$ mN/m, (b) $\pi_t = 35$ mN/m. The respective height profiles corresponding to the white line on the images are shown below.
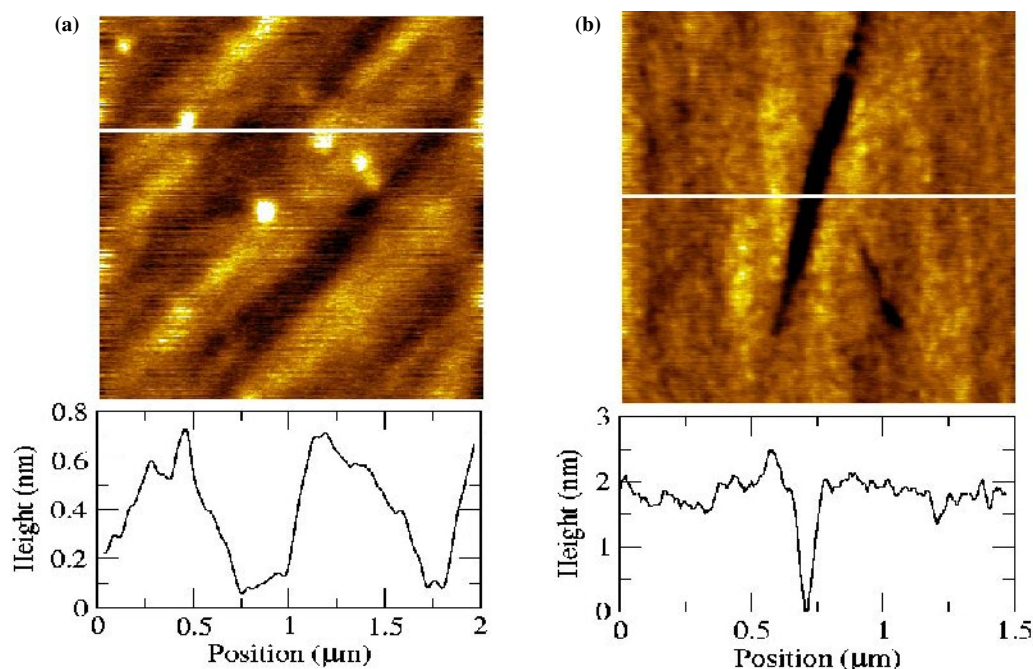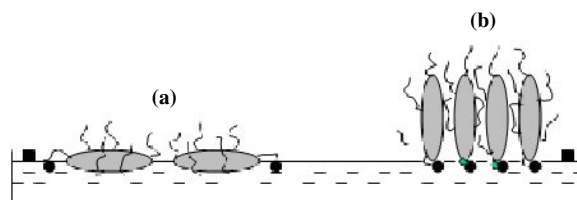

Figure 13: Schematic representation of the PyTp molecules in (a) face-on and (b) edge-on configuration at the A–W interface. [Reprinted with permission from reference 27. Copyright 2007 American Chemical Society].

substrate. Comparing with the molecular dimension, this value lies between the values expected for a face-on and an edge-on configuration of molecules in the film. The morphology of the film transferred at a π_t of 35 mN/m (Figure 15b) was compact and homogeneous with some small voids. The film showed a height of 3 ± 0.2 nm, which is more than the film height of pure PyTp in the edge-on configuration by nearly 1 nm. This extra thickness of 1 nm can be attributed to the presence of DNA in the film[40,41]. Comparing these and the surface manometry results with the

molecular dimension, we infer that the face-on configuration was suppressed. The phase transition was from loosely packed molecules in the edge-on configuration to a compactly packed edge-on configuration[28]. On the basis of these results, we have drawn a schematic diagram for the configuration of molecules at the A–W interface (Figure 16).

AFM topography for two layers of the PyTp–DNA complex LB film deposited at 35 mN/m on a hydrophobic silicon substrate are shown in Figure 17. As compared to the two layers of pure

Figure 14: AFM topography images of LB films of PyTp with two layers on hydrophobic silicon substrates transferred at different target surface pressures (π_t). Figures (a) $\pi_t = 35$ mN/m and (b) $\pi_t = 42$ mN/m show a morphology with narrow rectangular voids elongated in the film deposition direction. The respective height profiles corresponding to the lines drawn on the images are shown below.
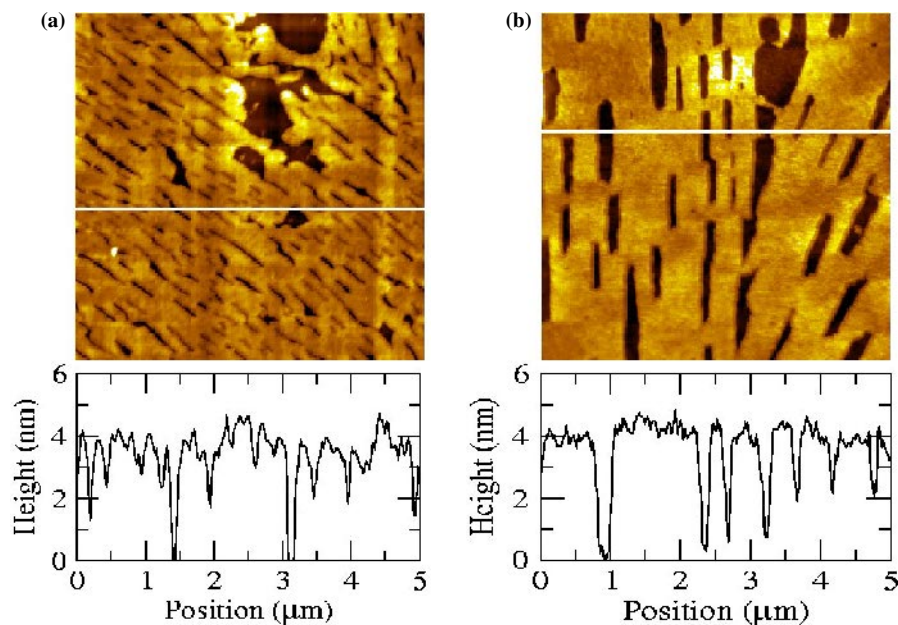

Figure 15: AFM images of a monolayer of the PyTp–DNA complex film transferred at (a) $\pi_t = 5$ mN/m and (b) $\pi_t = 35$ mN/m onto hydrophilic silicon substrates. The respective height profiles corresponding to the white lines on the images are shown below. [Reprinted with permission from reference 28. Copyright 2008 American Chemical Society].
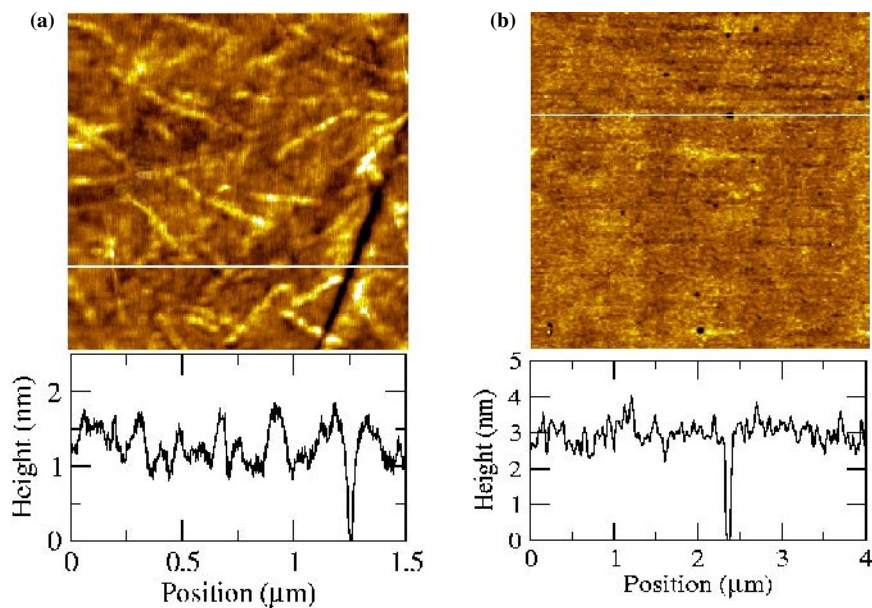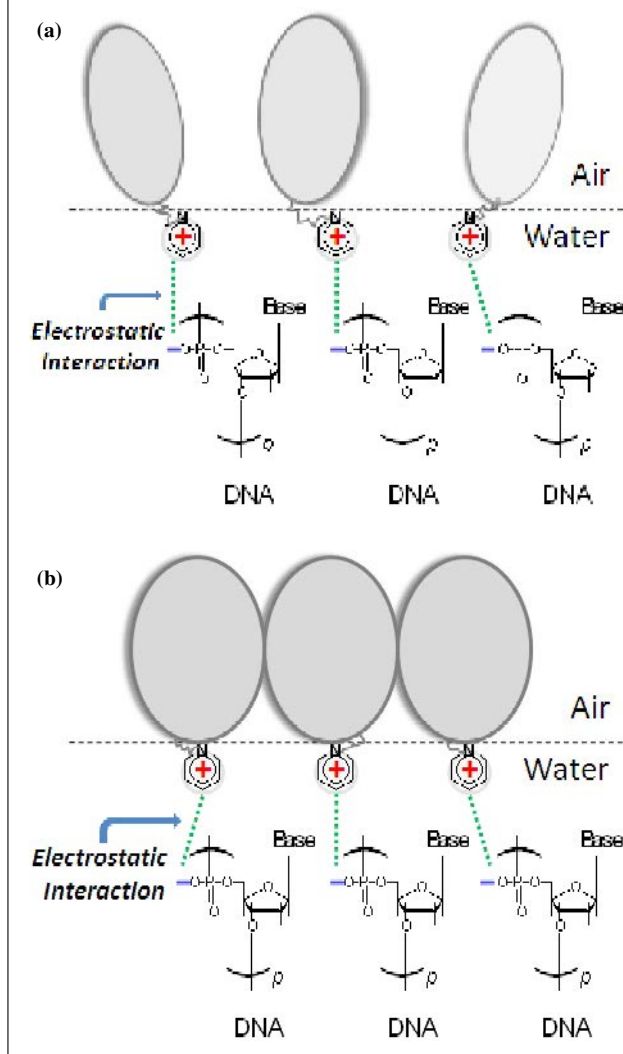
Figure 16: PyTp–DNA complex monolayer shown schematically in the edge-on configuration formed at the A–W interface. (a) Loosely packed molecules (A_o = 1.9 nm^2/molecule). (b) Compactly packed molecules (A_o = 0.9 nm^2/molecule). [Reprinted with permission from reference 28. Copyright 2008 American Chemical Society].

PyTp film which had regular rectangular voids, the morphology of the PyTp–DNA complex film with two layers was more compact, with some circular voids (Figure 17a) of different depth. To obtain the actual film thickness, we have scratched the film using an AFM tip in contact mode and then imaged the scratched region in tapping mode using the same tip (Figure 17b). The thickness of the film obtained by height profile across the scratch was 5 ± 0.5 nm.

We have studied the morphology and thickness of the complex films transferred up to 20 layers. The morphology of the complex film with 20 layers (Figure 18) showed thread-like structures aligned in the film deposition direction. These may be attributed to DNA bundles. The strong

Π–Π stacking interaction between the discotic cores brings multiple DNA strands together forming these thread-like bundles. Possible explanations for the alignment of these structures in the film deposition direction may be parallel alignment of the DNA strands at the A–W interface as well as the receding meniscus force during the transfer process. Our observation is consistent with the reports on the orientation of DNA strands along the dipping direction of LB films[42,43]. In the case of the pure PyTp film, it was not possible to transfer more than two layers efficiently. Interestingly, we find that the DNA complexation facilitated the film deposition of several tens of layers with high transfer ratio. Transfer ratio is a measure of the efficiency of film transfer onto a substrate. It is defined as the ratio

Figure 17: The AFM images for two layers of a PyTp–DNA complex film transferred at 35 mN/m onto hydrophobic silicon substrate. (a) Film surface showing circular voids. (b) Film surface showing the scratches to measure the thickness. The respective height profiles corresponding to the white lines on the images are shown below. [Reprinted with permission from reference 28. Copyright 2008 American Chemical Society].
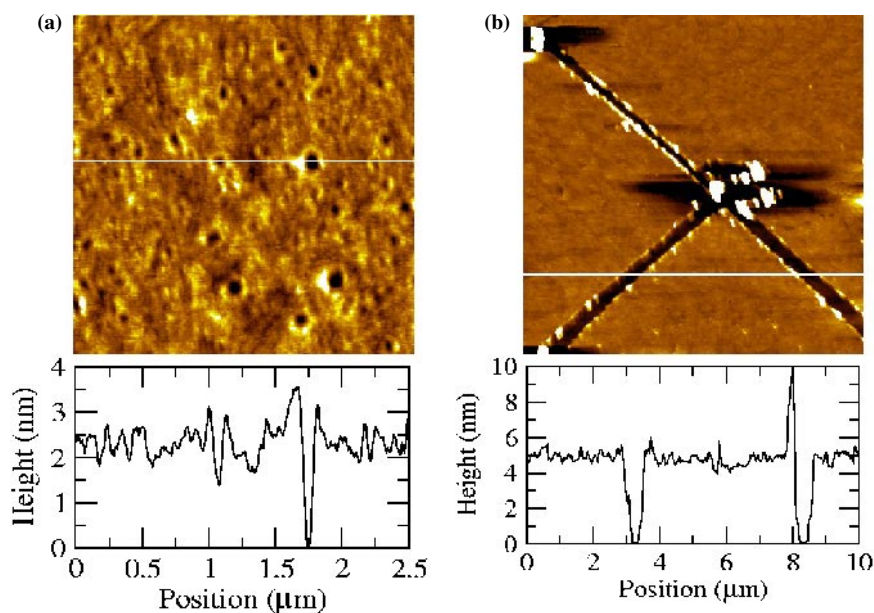
of decrease in Langmuir monolayer surface area to that of the total surface area of the substrate to be coated. Figure 19 shows the transfer ratio (τ) as a function of number of layers (n) of LB deposition upto 20 layers at a target surface pressure of 35 mN/m for PyTp–DNA complex film onto hydrophobic silicon substrate. The ability to transfer several layers provides a means to prepare ordered thin multilayer films for applications in electronic devices[5].

3.3.2. Current Images

Discotic mesogens are examples of organic semiconductors. The measurement of its electrical conductivity is important for device applications. We have carried out nanoscale electrical conductivity measurements for the PyTp monolayer film deposited on gold coated mica substrate by LB technique. The films were imaged by contact mode CS-AFM. By maintaining a constant force of 4 nN between the tip and sample, simultaneous topographic and current images were obtained for sample bias voltages of 1 and 2 V. For the sample bias voltage of 1 V, a current flow in the range of 0.1 to 0.4 nA was observed. The current features were further resolved by increasing the sample bias to 2 V. The simultaneously acquired topography and current images for pure PyTp monolayer film

at a bias voltage of 2 V are shown in Figures 20(a) and 20(b) respectively. At this bias voltage, a current flow of about 1 nA was observed through the film. The inhomogeneities observed in the current image might be due to the defects in the gold coating on mica substrate. Such inhomogeneities in current images are also reported in literature for organic films[33,34]. The PyTp–DNA complex monolayer film formed on gold coated mica substrate was also imaged by CS-AFM. As compared to PyTp film, the PyTp–DNA complex film exhibited measurable conductivity only above 1 V sample bias.

3.3.3. I–V Characteristics

We have performed the $I–V$ measurements at various positions on both the pure and complex films formed on gold coated mica substrates. The $I–V$ curves were acquired while the tip was held at a fixed position with a force of 4 nN and the applied voltage ramp was from -3 to $+3$ V with a scan rate of 1 Hz. The metal substrate, the film and the conducting tip form a nanoscopic metal-insulator-metal (M–I–M) junction as shown in Figure 21. Representative $I–V$ curves on pure film and complex film are shown in Figure 22(a) and 22(b) respectively. The tunneling current rapidly increased above a certain threshold voltage for both the films. For a given applied voltage, the value of

Figure 18: AFM topography images for 20 layers of PyTp–DNA complex film transferred at 35 mN/m onto hydrophobic silicon substrates. (a) Morphology of the film surface showing DNA bundles. (b) Scratched film to measure the thickness. The respective height profiles corresponding to the lines drawn on the images are shown below. [Reprinted with permission from reference 28. Copyright 2008 American Chemical Society].
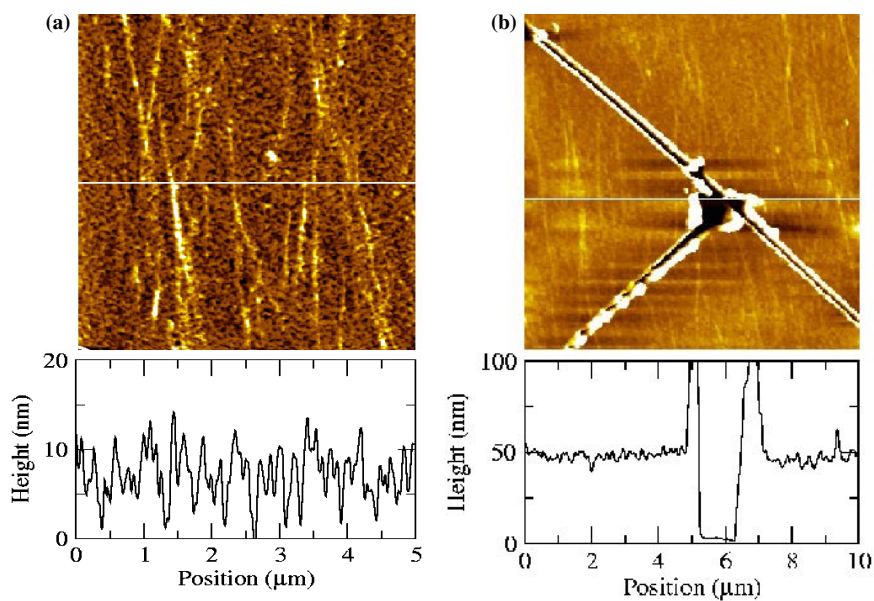

Figure 19: Transfer ratio (τ) as a function of number of layers (n) of LB deposition at a target surface pressure of 35 mN/m for PyTp–DNA complex film onto hydrophobic silicon substrate. Transfer ratio is a measure of the efficiency of film transfer onto a substrate. It is defined as the ratio of decrease in Langmuir monolayer surface area to that of the total surface area of the substrate to be coated.
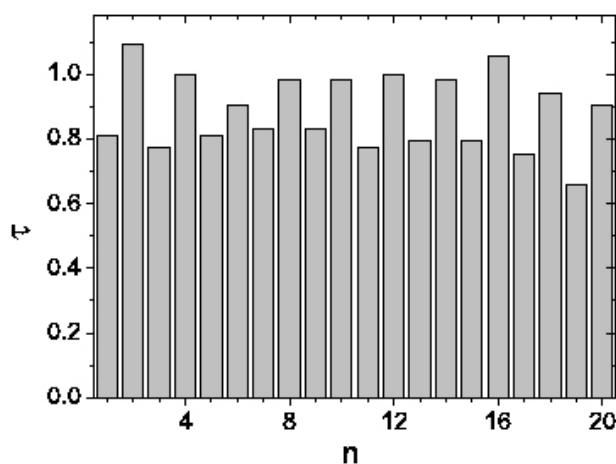
current for PyTp film was significantly larger than that for PyTp–DNA complex film. With an applied bias of 1 V, the average electrical currents through PyTp and PyTp–DNA complex films were 0.2 nA and 0.05 nA, respectively.

The shape of the I–V curves strongly suggests a barrier for electron transport at the tip–sample interface. The barrier height at the interface is an important parameter for electron transfer through the interface[44]. One can choose an appropriate model to describe the measured I–V curves and to determine the barrier height between the film and the metal substrate. We have considered two basic mechanisms for electron transport across a

Figure 20: CS-AFM images of the monolayer film of PyTp on gold coated mica substrate at a sample bias voltage of 2 V and a constant force of 4 nN : (a) Topography image showing the surface roughness. (b) Current image showing an average current of about 1 nA across the film. [Reprinted with permission from *Phys. Rev. E* (http://link.aps.org/doi/10.1103/PhysRevE.78.021606), reference 29. Copyright 2008 by the American Physical Society].
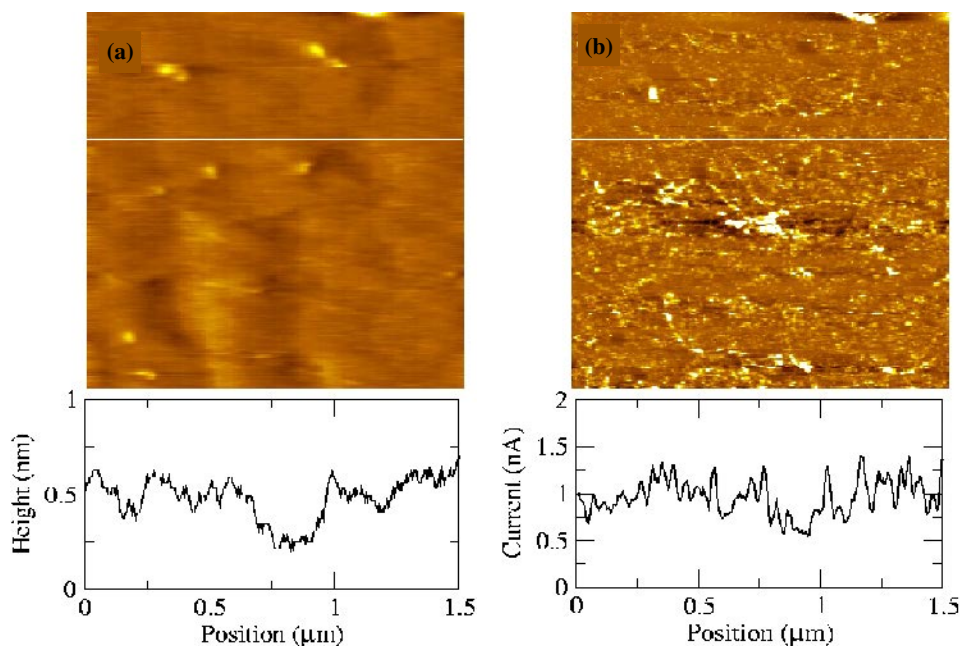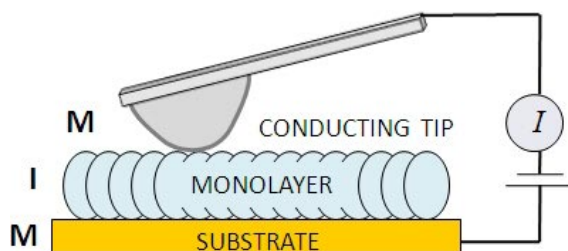

Figure 21: Metal–insulator–metal (M–I–M) junction drawn schematically for a conducting AFM tip in contact with a monolayer film deposited on a conducting substrate.

potential barrier; thermionic emission (Schottky emission) and electron tunneling[45]. Thermionic emission can occur when the electrons have enough energy to pass over the potential barrier. In the thermionic emission model for a M–I–M junction, the derivative dI/dV decreases with increasing current. In our systems, dI/dV increases with increasing current in the measured I–V curves. Therefore, the nature of the I–V curves suggests that the electron tunneling is the possible mechanism for electron transport in our system. For interpreting electron tunneling, Fowler–Nordheim (FN) model is widely used[46,47]. This model describes the electron tunneling from a metal's Fermi level over a barrier into an adjacent material.

For a M–I–M structure, the FN tunneling current is given by the following equation[48,49],

$$I = \frac{A_{\text{eff}}q^3E^2m}{8\pi h\phi_b m^*}\exp\left[\frac{-8\pi\sqrt{2m^*}\phi_b^{3/2}}{3hqE}\right] \quad (1)$$

where A_{eff} is the effective contact area, E is the applied electric field, ϕ_b is the contact barrier height, and q, m^*, m, and h are electron charge, effective

Figure 22: Current–voltage curves obtained by CS-AFM on monolayer films of (a) PyTp and (b) PyTp–DNA complex, on gold coated mica substrates at a constant force of 4 nN. The solid circles represent forward voltage scan and the open circles represent reverse voltage scan. [Reprinted with permission from *Phys. Rev. E* (http://link.aps.org/doi/10.1103/PhysRevE.78.021606), reference 29. Copyright 2008 by the American Physical Society].
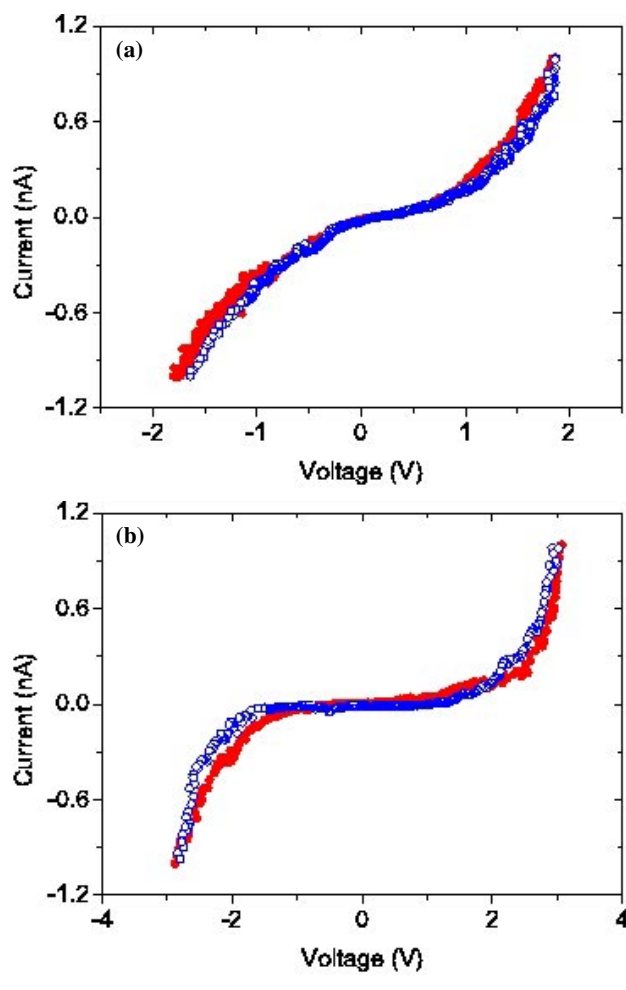
mass of the electron, free electron mass, and Plank constant, respectively. If we assume $E = V/d$, where V is the applied voltage, and d is the separation between the two electrodes, then

$$I = AV^2 \exp\left(\frac{-B}{V}\right) \qquad (2)$$

where

$$A = \frac{A_{eff}q^3 m}{8\pi h \phi_b d^2 m^*} \qquad (3)$$

and

$$B = \frac{8\pi\sqrt{2m^*}\phi_b^{3/2}d}{3hq} = 6.83d\left(\frac{m^*}{m}\right)^{1/2}\phi_b^{3/2}. \qquad (4)$$

Here the units of B, d and ϕ_b are Volts, nm and eV, respectively. In our system, the separation between the two electrodes (d) is the distance between the probe and the gold substrate. Since the tip of the probe is located just at the surface of the LB film, d is nearly equal to the thickness of the film[50].

We have used the B value calculated from equation 4 for extracting the barrier heights for both the pure and complex monolayer films[46]. We have fitted the $I–V$ data for the pure and complex monolayer films with the FN model i.e., equation 2. Figures 23(a) and 23(b) show the FN plot of $\ln(I/V^2)$ against $1/V$ for the pure and complex films, respectively. The FN plot shows a straight line whose slope yields the B value. The open circles represent the experimental data points and the solid

Figure 23: Fowler–Nordheim fitting to typical current–voltage (I–V) curves measured for (a) pure PyTp monolayer film, and (b) PyTp–DNA complex monolayer film, at a constant force of 4 nN. Open circles represent the experimental data and solid line represents the fit. [Reprinted with permission from *Phys. Rev.E* (http://link.aps.org/doi/10.1103/PhysRevE.78.021606), reference 29. Copyright 2008 by the American Physical Society].
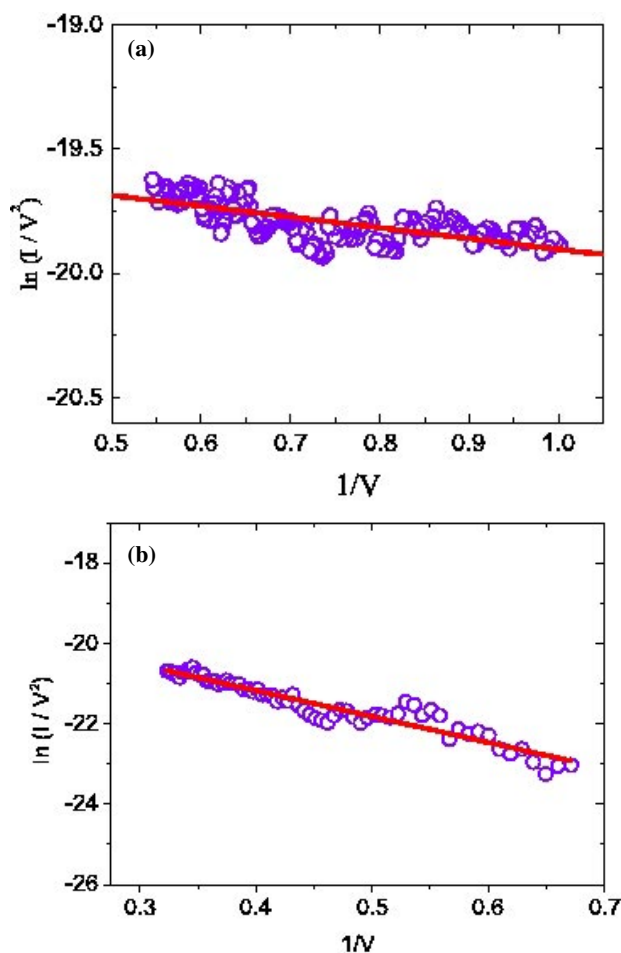
line represents the fit. We find that the I–V data for both the films fit well with this model. It is to be noted that FN is an approximation in the high voltage regime. Therefore, we have shown the fitting of our data for the high voltage regime only. At lower voltages, the system charging effect, thermal and Schottky effects become dominant which deprives us from extracting any meaningful information at that regime. On the basis of our analysis and within our experimental limits, we find FN to be a possible mechanism for electron transport in our system. We have obtained several I–V curves at different positions of the tip on the films and fitted them with the FN model. The average B values obtained from such measurements

were 0.85 V for the pure film and 6.6 V for the complex film. The film thicknesses were 2.2 nm for PyTp and 3.2 nm for PyTp–DNA complex. Using the average B values and the corresponding film thicknesses in equation 4, we have calculated the barrier heights, ϕ_b, to be $0.15(m/m^*)^{1/3}$ eV and $0.45(m/m^*)^{1/3}$ eV for the pure and complex films, respectively. These results suggest that for the pure film the barrier height may be as low as 0.15 eV. For PyTp–DNA complex system, we find that the presence of DNA leads to a larger barrier to electron transport. The higher barrier height is likely to be a direct consequence of change in packing of the molecules. The conformation of DNA molecule and the environment in which it is present have a strong

influence on its conductivity[19]. On the basis of our observations, we find that complexation with DNA makes the film more resistive.

4. Conclusions

Ionic discotic liquid crystals exhibit interesting electronic properties and find applications in the fabrication of many electronic devices. We have studied films of pyridinium salt tethered with hexaalkoxytriphenylene (PyTp) at air–water and air–solid interfaces. PyTp molecules exhibited stable monolayer at air–water. As compared to the monolayers of non-ionic triphenylene derivatives reported so far, these cationic discotic liquid crystalline molecules showed higher limiting area per molecule due to the direct electrostatic repulsion between the molecules within the film. The surface manometry, Brewster angle microscope and atomic force microscope (AFM) studies indicate a phase transition from a face-on configuration to an edge-on configuration. The presence of a cationic moiety in the PyTp molecule opens the scope for studying electrostatic interaction with other molecules at interfaces. We have formed the PyTp monolayer on a subphase containing small amount of DNA molecules. This results in a supramolecular complexation between DNA and PyTp, at air–water interface. The complex formation is primarily due to the electrostatic interaction between the pyridinium group of the discotic molecule and the phosphate group of DNA. The complex yields a monolayer with an increased collapse pressure indicating much higher stability. Also, we find that the face-on molecular configuration exhibited by the PyTp monolayer is suppressed and the complex exhibits a phase transition from a loosely packed edge-on configuration to a compactly packed edge-on molecular configuration. The transfer of the complex monolayer onto substrates by Langmuir–Blodgett (LB) technique becomes much more efficient compared to that of pure monolayer. It was possible to transfer several tens of layers with good transfer ratio. The efficiency of the PyTp–DNA complex to form multilayers on a substrate can find applications in devices such as thin film transistors and nucleic acid based biosensors. For fabrication of electronic devices, measurement of conductivity is very important. Employing a current sensing atomic force microscope, we have measured the nanoscale electrical conductivity of LB films of PyTp and PyTp–DNA complex. The current–voltage ($I–V$) characteristics strongly suggests a barrier for electron transport at the AFM cantilever tip–film interface. Further, the $I–V$ curves fit well with the Fowler–Nordheim (FN) model indicating the electron tunneling to be the most probable mechanism for electron transport through the monolayer. We find the barrier of PyTp–DNA complex film to be three times higher compared to that of the pure PyTp film indicating that complexation of PyTp with DNA makes the film more resistive.

References
1. J. Y. Josefowicz, N. C. Maliszewskyj, S. H. J. Idziak, P. A. Heiney, J. P. McCauley, and A. B. Smith, *Science* **260**, 323 (1993).
2. R. Ionov and A. Angelova, *Phy. Rev. E* **52**, 21(R) (1995).
3. D. Gidalevitz, O. Y. Mindyuk, P. A. Heiney, B. M. Ocko, P. Henderson, H. Ringsdorf, N. Boden, R. J. Bushby, P. S. Martin, J. Strzalka, J. P McCauley, and A. B. Smith, *J. Phys. Chem. B* **101**, 10870 (1997).
4. A. D. Dunbar, T. M. Richardson, A. J. McNaughton, J. Hutchinson, and C. A. Hunter, *J. Phys. Chem. B* **110**, 16646 (2006).
5. W. Pisula, A. Menon, M. Stepputat, I. Lieberwirth, U. Kolb, A. Tracz, H. Sirringhaus, T. Pakula, and K. Mullen, *Adv. Mater.* **17**, 684 (2005).
6. J. P. Schmidtke and R. H. Friend, *J. Chem. Phys.* **124**, 174704 (2006).
7. S. Kumar and S. K. Varshney, *Angew. Chem. Int. Ed.* **39**, 3140 (2000).
8. M. Van der Auweraer *et al. Thin Solid Films* **210/211**, 39 (1992).
9. C. A. Hunter and J. K. M. Sanders, *J. Am. Chem. Soc.* **112**, 5525 (1990).
10. N. C. Maliszewskyj, P. A. Heiney, K. J. Blasie, J. P. McCauley, and A. B. Smith, *J. Phys. II France* **2**, 75 (1992).
11. G. Roberts, *Langmuir–Blodgett Films*, Plenum Press: New York, (1990).
12. K. Binnemans, *Chem. Rev.* **105**, 4148 (2005).
13. M. Yoshio, T. Mukai, H. Ohno, and T. Kato, *J. Am. Chem. Soc.* **126**, 994 (2004).
14. C. M. Gordon, J. D. Holbrey, A. R. Kennedy, and K. R. Seddon, *J. Mater. Chem.* **8**, 2627 (1998).
15. Sandeep Kumar *Chem. Soc. Rev.* **35**, 83 (2006).
16. S. Sergeyev, W. Pisula, and Y. H. Geerts, *Chem. Soc. Rev.* **36**, 1902 (2007).
17. D. Porath, A. Bezryadin, S. de Vries, and C. Dekker, *Nature* **403**, 635 (2000).
18. L. Cai, H. Tabata, and T. Kawai, *Appl. Phys. Lett.* **77**, 3105 (2000).
19. R. G. Endres, D. L. Cox, and R. R. P. Singh, *Rev. Mod. Phys.* **76**, 195 (2004).
20. L. Cui, J. Miao, and L. Zhu, *Macromolecules* **39**, 2536 (2006).
21. L. Cui and L. Zhu, *Langmuir* **22**, 5982 (2006).
22. M. P. W. Frances, L. R. Dorothy, and B. B. Marcel, *Biochemistry* **35**, 5756 (1996).
23. M. Sastry, V. Ramakrishnan, M. Pattarkine, A. Gole, and K. N. Ganesh, *Langmuir* **16**, 9142 (2000).
24. J. O. Radler, I. Koltover, T. Salditt, and C. R. Safinya, *Science* **275**, 810 (1997).
25. G. B. Sukhorukov, M. M. Montrel, A. I. Petrov, L. I. Shabarchina, and B. I. Sukhorukov, *Biosens. Bioelectron.* **11**, 913 (1996).

26. C. Symietz, M. Schneider, G. Brezesinski, and H. Möhwald *Macromolecules* **37**, 3865 (2004).

27. A. Nayak, K. A. Suresh, S. K. Pal, and S. Kumar, *J. Phys. Chem. B* **111**, 11157 (2007).

28. A. Nayak and K. A. Suresh, *J. Phys. Chem. B* **112**, 2930 (2008).

29. A. Nayak and K. A. Suresh, *Phys. Rev. E* **78**, 021606 (2008).

30. N. P. Guisinger, N. L. Yoder, and M. C. Hersam, *Proc. Natl. Acad. Sci. U.S.A* **102**, 8838 (2005).

31. D. J. Wold and C. D. Frisbie, *J. Am. Chem. Soc.* **122**, 2970 (2000).

32. M. Freitag, M. Radosavljevic, W. Clauss and A. T. Johnson, *Phys. Rev. B* **62**, R2307 (2000).

33. X. D. Cui, X. Zarate, J. Tomfohr, O. F. Sankey, A. Primak, A. L. Moore, T. A. Moore, D. Gust, G. Harris, and S. M. Lindsay, *Nanotechnology* **13**, 5 (2002).

34. D. -H. Han, J. -W. Kim, and S. -M. Park, *J. Phys. Chem. B* **110**, 14874 (2006).

35. J. M. Beebe, B. S. Kim, J. W. Gadzuk, C. D. Frisbie, and J. G. Kushmerick, *Phys. Rev. Lett.* **97**, 026801 (2006).

36. S. Kumar and S. K. Pal, *Tetrahedron Lett.* **46**, 4127 (2005).

37. M. Broniatowski, I. Sandez Macho, Jr. J. Minones, and P. Dynarowicz-Latka, *J. Phys. Chem. B* **108**, 13403 (2004).

38. J. T. Davies and E. K. Rideal, *Interfacial Phenomena*, Academic Press: New York, (1963).

39. O. Y. Mindyuk and P. A. Heiney, *Adv. Mater.* **11**, 341 (1999).

40. J. C. Wu, T. L. Lin, U. S. Jeng, H. Y. Lee, and T. Gutberlet, *Physica B* **385**, 841 (2006).

41. K. Kago, H. Matsuoka, R. Yoshitome, H. Yamaoka, K. Ijiro, and M. Shimomura, *Langmuir* **15**, 5193 (1999).

42. Y. Okahata, T. Kobayashi, and K. Tanaka, *Langmuir* **12**, 1326 (1996).

43. A. Bhaumik, M. Ramakanth, L. K. Brar, A. K. Raychaudhuri, F. Rondelez, and D. Chatterji, *Langmuir* **20**, 5891 (2004).

44. I. Casuso, L. Fumagalli, J. Samitier, E. Padros, L. Reggiani, V. Akimov, and G. Gomila, *Phys. Rev. E* **76**, 041919 (2007).

45. D. Xu, G. D. Watt, J. N. Harb, and R. C. Davis, *Nano Lett.* **5**, 571 (2005).

46. A. Olbrich, B. Ebersberger, and C. Boit, *Appl. Phys. Lett.* **73**, 3114 (1998).

47. I. Casuso, L. Fumagalli, J. Samitier, E. Padros, L. Reggiani, V. Akimov, and G. Gomila, *Nanotechnology* **18**, 465502 (2007).

48. J. G. Simmons, *J. Appl. Phys.* **34**, 1793 (1963).

49. M. Lenzlinger and E. H. Snow, *J. Appl. Phys.* **40**, 278 (1969).

50. K. Yano, M. Kyogaku, R. Kuroda, Y. Shimada, S. Shido, H. Matsuda, K. Takimoto, O. Albrecht, K. Eguchi, and T. Nakagiri, *Appl. Phys. Lett.* **68**, 188 (1996).

Alpana Nayak is a Post-Doctoral Researcher at the National Institute for Materials Science,Tsukuba,Japan. Formerly, she was a Senior Research Fellow at the Raman Research Institute, Bangalore. Her research interests are soft condensed matter, liquid crystals, thin organic films at interfaces, scanning probe microscopy and nano-electronic devices.

Kattera A. Suresh is presently the Director at the Centre for Liquid Crystal Research, Bangalore and before that he was a Senior Professor at the Raman Research Institute, Bangalore. His research interests are in the physics of liquid crystals, surface and interfacial science, thin films and complex fluids.